Proceedings of the 69th International Astronautical Congress 2018 (IAC '18),
1-5 October 2018, Bremen, Germany.
https://iafastro.directory/iac/paper/id/43727/summary/

Gauss' Variational Equations for Low-Thrust Optimal Control Problems in Low-Energy Regimes

Rita Neves[a]*, **Joan-Pau Sánchez**[a]

[a] *School of Aerospace, Cranfield University, College Road, Cranfield MK43 0AL, United Kingdom*, {r.neves, jp.sanchez}@cranfield.ac.uk
* Corresponding Author

Abstract

This paper proposes a new description of the equations of motion for low-thrust trajectory design in the presence of a third-body perturbation. The framework is formulated using Gauss' Variational Equations (GVE) with two distinct accelerations: the one produced by the electric engine and the disturbing term of the third-body effect. The latter is computed using the disturbing potential of the previously studied Keplerian Map, formulated from the Hamiltonian of the circular-restricted three-body problem. The presented GVE framework is advantageous in several respects: first, low-thrust sub-optimal control laws can be easily generated and explored to find a first guess solution near global optima. Second, bounds for the optimal control problem, as well as boundary values, can be easily defined, leading to a much faster convergence. This dynamical framework is accurate until very close to the sphere of influence of the perturbing body, and thus can be efficiently used to target low-energy hyperbolic invariant manifold structures associated with periodic orbits near it. This paper presents the methodology as well as a full retrieval trajectory for asteroid 2018 AV2, a small co-orbital asteroid that could be retrieved during its next Earth encounter in 2037.
Keywords: Low-thrust; Optimal control problem; Trajectory design; Optimisation; Asteroid capture

Nomenclature

μ: Normalized gravitational parameter
$\mathcal{R}$: Disturbing function
$\mathcal{U}_{3B}$: Keplerian Third-Body Potential
C: Jacobi Constant
v_∞: Escape Velocity

Acronyms

Near-Earth asteroid (NEA)
Libration point orbit (LPO)
Keplerian Map (KM)
Gauss' Variational Equations (GVE)
Circular-Restricted Three-Body Problem (CR3BP)

1. Introduction

With the pursuit of increasingly innovative and complex space missions, the focus of the space industry has been turning towards low-thrust technologies. Electric propulsion systems provide large savings in propellant mass, which can be decisive for the mission's feasibility: the higher the entire system's mass is, the costlier the endeavour will be, making it less likely to come into fruition. Since the first spacecraft using low-thrust was successfully flown in 1999 [1], this technology has allowed for the planning of a range of missions that would otherwise be infeasible, including visits to the outer planets, comets and asteroids [2].

Designing a low-thrust trajectory is a more complex task than doing so for a high-thrust one. For the latter case, the few short thrust phases can be approximated by singular events that change the spacecraft's velocity instantaneously. On the contrary, low-thrust missions require the propulsion system to operate for a significant part of the transfer, in order to generate the necessary velocity increment. Consequently, the thrust vector is a continuous function of time and the trajectory optimisation problem has to find the optimal control strategy [3]. This is an extremely complex problem that has no closed-form solutions, except for some very specific cases [4]. Thus, the optimal control problem has to be carefully conceived in order to achieve convergence, i.e. a meaningful definition of bounds and constraints for the trajectory is necessary.

One of the main steps in the formulation of the optimal control problem is choosing the model of motion in which the trajectory is developed [5]. Certain design applications, like missions to near-Earth asteroids (NEA) require models of motion of higher complexity than the classical two-body problem. Using an alternative higher-fidelity method, such as the circular restricted three-body problem (CR3BP), has certain drawbacks that relate to the complexities in defining the optimal control problem, e.g. boundary conditions are hard to set since the coordinates are presented in the synodic cartesian reference frame.

Thus, this paper proposes a new set of equations to

model third-body motion that may be accelerated by a low-thrust engine. These are obtained by propagating Gauss' Variational Equations (GVE) with the sum of two disturbing acceleration vectors. The first is obtained from the thrust produced by the electric engine; the second corresponds to the third-body perturbation. The latter is derived from the Keplerian Third-Body Potential of the previously studied Keplerian Map (KM) [6, 7].

In this paper, the framework of the GVE is applied to bodies moving in *low-energy regimes*. The latter is here defined as the regime of motion in which ballistic capture is theoretically possible [8]: this may occur for objects whose orbital energy does not differ much from that of the third-body perturbation, e.g. nearly co-orbital bodies [9] or spacecraft departing from or arriving to Earth with a low v_∞. An example of a low-energy regime trajectory is the low-thrust capture of NEA [10]. Thus, a test example of the usability of these equations is presented with the design of such a capture transfer. For this purpose, a simple mission is formulated: a spacecraft attaches itself to an asteroid and moves it from its nominal orbit to one of the invariant manifolds of the Sun-Earth system, connected to a Planar Lyapunov orbit.

The structure of this paper is set as follows: Section 2 provides a brief summary of well-known models of motion that will be used for comparison. Section 3 presents the framework for the GVE equations using the Keplerian Third-Body Potential, as well as the derivations of the relevant accelerations. Section 4 details the steps involved in the design of a first guess low-thrust trajectory. Section 5 highlights the results of the trajectory design for the chosen NEA, and Section 6 concludes the paper with final considerations and future work.

2. Classical Models of Motion

The problem of predicting the trajectory of a body in space requires the choice of an adequate model of motion. Throughout time, several methods have been used to this purpose, depending on the problem. Some classical models will be used as comparison methods to the GVE equations presented on this paper: these are revised below.

2.1 Circular Restricted Three-Body Problem

Throughout this paper, the gravitational interactions to be considered on the spacecraft will be those of the Sun and the Earth: a three-body problem. The CR3BP is a simplification on the latter, in which the third body's mass is deemed insignificant when compared to the other two, the primaries, and their orbits are circular around each other. The normalised position and velocity in the CR3BP obey the following equations of motion, in the synodic reference frame [11]:

$$\begin{aligned}
\ddot{x} - 2\dot{y} - x &= -\frac{(1-\mu)(x+\mu)}{{r_1}^3} - \frac{\mu(x-1+\mu)}{{r_2}^3} \\
\ddot{y} + 2\dot{x} - y &= -\frac{(1-\mu)y}{{r_1}^3} - \frac{\mu y}{{r_2}^3} \\
\ddot{z} &= -\frac{(1-\mu)z}{{r_1}^3} - \frac{\mu z}{{r_2}^3}
\end{aligned} \tag{1}$$

where r_1 and r_2 are the distances to each of the primaries and $\mu = \frac{m_2}{m_1+m_2}$ is the normalised gravitational parameter of the system, given that m_1 and m_2 are the masses of the primary and secondary.

2.1.1 Dynamical Structures

The equations of motion of the CR3BP admit five equilibrium solutions, known as the libration points $L_i, i = 1, 2, ...5$. In their vicinity, one can find the libration point orbits (LPOs): these are characterized by a motion that repeats itself after a time period, as seen relative to the synodic reference frame. Given that these orbits are not stable, one can find invariant manifold structures connected to them. Geometrically, these are tubes that depart from or arrive to the periodic orbit.

The aforementioned dynamical structures make it so that, if a spacecraft is inserted into an invariant manifold orbit, it will end up in a periodic orbit without any fuel expenditure. This is only possible due to the simultaneous gravitational interactions between the primaries (Sun and Earth, as selected in this paper), which have to be carefully considered when designing trajectories.

2.2 Multi-Body Dynamics

The motion of an object in an environment where many celestial bodies are gravitationally interacting with each other is described by the $n - bodyproblem$. This is formulated by Equation 3, which cannot be solved for more than two bodies without resorting to approximations like the CR3BP described above.

$$\ddot{\vec{r}}_{SC} = -\mu_i \cdot \frac{\vec{r}_i}{r_i^3} + \sum_{\substack{j=1 \\ j\neq i}}^{N-1} \left[\mu_j \left(\frac{\vec{r}_j - \vec{r}_i}{(r_j - r_i)^3} - \frac{\vec{r}_j}{r_j^3} \right) \right], \tag{2}$$

$$j, i = 0, ..., N-1 \tag{3}$$

in which $\vec{r_{SC}}$ is the position vector of the spacecraft, i is the index of the central body, j is the index of each remaining one and μ is the gravitational parameter related to the celestial object.

Equation 3 implies that, in the Sun-Earth system, even when outside the sphere of influence of the Earth, the

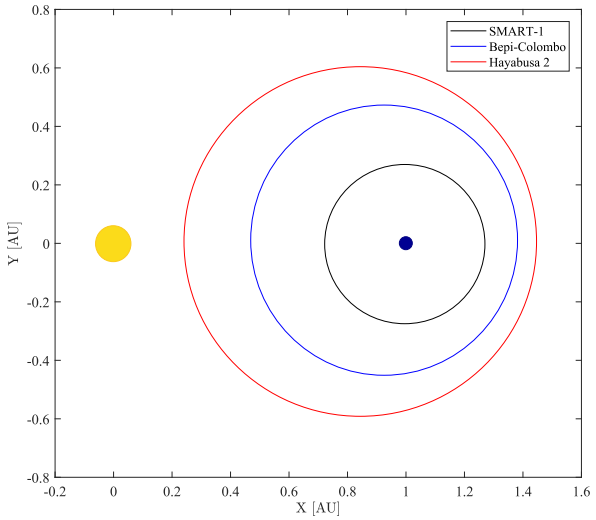

Fig. 1: Regions where each spacecraft acceleration is comparable to the one of the Earth. Earth represented with the size of its sphere of influence

spacecraft is affected by its perturbation. In the current paper, this zone is referred to as the *perturbation region*: an area in the Earth's vicinity where its acceleration affects the third-body's trajectory substantially, rendering the two-body problem inaccurate. This is here delimited as a the region between the sections forming an angle of $\pm\pi/8$ with the Sun-Earth line, as defined by Sánchez and Yárnoz [12].

In order to further support the claim above, the accelerations of the Earth on a hypothetical third-body were computed with Equations 3, as a function of the third-body's position. Then, these were compared to the output accelerations of three different spacecraft with electrical engines: SMART-1, Bepi-Colombo and Hayabusa 2. For each of these, Figure 1 shows the regions in which their accelerations were at most 1000 times greater than the Earth's perturbation, a threshold in which the latter is considered to be significant in the trajectory design. Naturally, these areas will change with the low-thrust system considered; however, it is clear that the Earth's disturbing acceleration is non-negligible within a much larger region than the classical sphere of influence.

3. Gauss' Variational Equations' Framework

This section presents the development of the GVE framework for low-thrust design in low-energy regimes, from the derivation of the disturbing accelerations to the reference frame rotations and final propagation flowchart.

3.1 Equations of Motion

Gauss' Variational Equations (GVE) have been extensively used in astrodynamics to compute motion perturbed by a disturbing acceleration. Following Battin [13], they can be formulated in this manner:

$$\begin{aligned}
\frac{da}{dt} &= \frac{2a^2}{h}\left(a_r e\sin\nu + a_\theta\frac{p}{r}\right)\\
\frac{de}{dt} &= \frac{1}{h}\Big(a_r p\sin\nu + a_\theta((p+r)\cos\nu + re)\Big)\\
\frac{di}{dt} &= a_h\frac{r\cos\theta}{h}\\
\frac{d\Omega}{dt} &= a_h\frac{r\sin\theta}{h\sin i}\\
\frac{d\omega}{dt} &= \frac{1}{he}\Big(-a_r p\cos\nu + a_\theta(p+r)\sin\nu\Big)\\
&\quad - a_h\frac{r\sin\theta\cos i}{h\sin i}\\
\frac{d\nu}{dt} &= \frac{h}{r^2} + \frac{1}{he}\Big(a_r p\cos\nu - a_\theta(p+r)\sin\nu\Big)
\end{aligned} \tag{4}$$

in which h is the angular momentum, p is the semilatus rectum, b is the semi-minor axis, r is the orbital position and $\theta = \nu + \omega$ is the argument of latitude, with ν as the true anomaly.

In contrast to the Lagrange Planetary Equations, GVE can also account for non-conservative accelerations. Consequently, they are especially useful in the case of a low-thrust spacecraft moving in a three-body configuration. The accelerations in that particular scenario are represented by Equation 5.

$$a_{GVE} = \{a_r, a_\theta, a_h\} = a_{LT} + a_{U3B} \tag{5}$$

Per Newton's first law, a_{LT} is easily computed as the quotient of the thrust vector and the system's mass. The vector a_{U3B} is here computed using the Keplerian Third-Body Potential of the Keplerian Map [6, 7], a method to compute the evolution of orbital parameters in a low-energy regime. This model is valid for planetary systems where the normalised gravitational parameter is very small, as is the case of the Sun-Earth system example.

3.2 The Keplerian Third-Body Potential

The three-body planetary system from which the disturbing potential function is derived can be seen on Figure 2. The main quantities are here represented, together with a new element: Ω_{Rot}, which is the rotational longitude of the ascending node of the spacecraft. This is defined in such a way that the inertial system's x-axis is aligned with the Earth [7]. It is worth noting that the movement is not made in the synodic reference frame: it is inertial, Sun-centred, but measured from the Earth axis (hence called

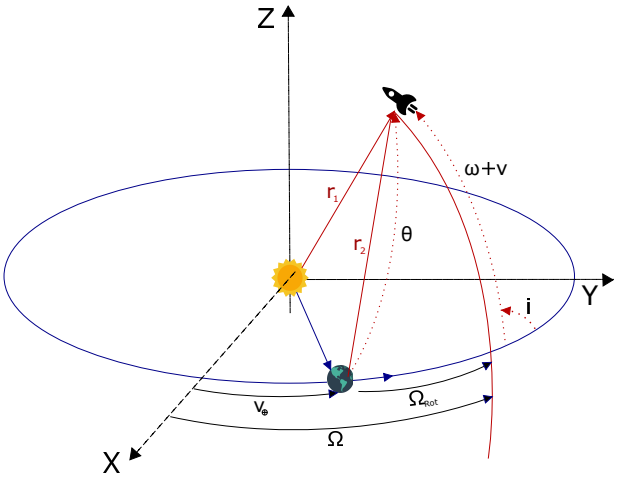

Fig. 2: Three-dimensional geometry of the three-body problem in the inertial reference frame

Earth-pointing reference frame). Thus, Ω_{Rot} replaces the regular Ω in Equations 4; it is computed using the initial longitude of the ascending node Ω_0, the true anomaly of the Earth and its initial value $\nu_\oplus^0$:

$$\Omega_{Rot} = \Omega_0 - \nu_\oplus - \nu_\oplus^0 \tag{6}$$

Finding the true anomaly of the Earth $\nu_\oplus$ for every step of the propagation could be a cumbersome task; thus, its value is approximated considering a circular Earth motion. Thus, the mean, eccentric and true anomalies of the Earth the same and the following relations are derived:

$$\begin{aligned} M_\oplus &= E_\oplus = \nu_\oplus \\ M_\oplus &= n_\oplus (t - t_0) \\ \nu_\oplus &= t - t_0 \end{aligned} \tag{7}$$

in which $n_\oplus$ is the Earth's mean motion, approximated to 1. Thus, the true anomaly of the Earth can be estimated from the normalized time of the propagation.

In order to generate a_{U3B} for Equations 5, the Hamiltonian of the CR3BP is formulated in this Earth-pointing reference frame, as previously done by Alessi and Sánchez [7]:

$$\mathcal{H}_{3B} = \frac{1}{2}(p_x^2 + p_y^2 + p_z^2) - \frac{1-\mu}{r_1} - \frac{\mu}{r_2} \tag{8}$$

in which r_1 and r_2 are the distances from the third body to the primary and secondary, respectively.

The first step is to write r_1 and r_2 as functions of the distance to the barycentre r. As a first step, the following equations are obtained:

$$r_1^2 = (x+\mu)^2 + y^2 + z^2 \tag{9}$$
$$r_2^2 = (x-1+\mu)^2 + y^2 + z^2 \tag{10}$$

Using polar coordinates $\{x = r\cos\theta; \sqrt{y^2+z^2} = r\sin\theta\}$:

$$r_1^2 = (r\cos\theta + \mu)^2 + (r\sin\theta)^2 \tag{11}$$
$$r_2^2 = (r\cos\theta - 1 + \mu)^2 + (r\sin\theta)^2 \tag{12}$$

Starting with the development of r_1 into a function of r,

$$\begin{aligned} r_1^2 &= r^2 + \mu^2 + 2r\mu\cos\theta \Leftrightarrow \\ \Leftrightarrow \frac{1}{r_1} &= \frac{1}{r}\frac{1}{\sqrt{1 + 2\cos\theta\frac{\mu}{r} + (\frac{\mu}{r})^2}} \end{aligned} \tag{13}$$

Assuming a Taylor expansion around $\mu = 0$ for the terms with r_1 and r_2:

$$\frac{1-\mu}{r_1} \approx \frac{1}{r} + \mu\Big(-\frac{1}{r} - \frac{\cos\theta}{r^2}\Big) + \mathcal{O}(\mu^2) \tag{14}$$
$$\frac{\mu}{r_2} \approx \frac{\mu}{\sqrt{r^2 - 2r\cos\theta + 1}} + \mathcal{O}(\mu^2) \tag{15}$$

It is important to denote that the Taylor expansions done on the previous equations imply that $\mu \ll r$. This means that, ultimately, the location of the primary and the barycentre cannot be distinguished: thus, the parameters corresponding to Equation 14 bear little impact on the final formulation of the Hamiltonian in Equation 16.

Finally, the Hamiltonian can be written as the sum of the kinetic and the potential energies:

$$\mathcal{H}_{3B} = \mathcal{K}_{3B} + \mathcal{U}_{3B} + \mathcal{O}(\mu^2) \tag{16}$$

in which:

$$\mathcal{K}_{3B} = \frac{1}{2}(p_x^2 + p_y^2 + p_z^2) - \frac{1}{r} \tag{17}$$
$$\mathcal{U}_{3B} = \mu\left(\frac{1}{r} + \frac{\cos\theta}{r^2} - \frac{1}{\sqrt{1 + r^2 - 2r\cos\theta}}\right) \tag{18}$$

where the physical quantities r and $\cos\theta$ are simply defined in the Earth-pointing reference frame:

$$\begin{aligned} r &= \sqrt{x^2 + y^2 + z^2} \\ \cos\theta &= \frac{x}{r} \end{aligned} \tag{19}$$

Using Hamiltonian mechanics, the third-body accelerations are computed as in Equation 20:

$$\begin{aligned} a_x &= -\frac{\partial \mathcal{U}_{3B}}{\partial x} \\ a_y &= -\frac{\partial \mathcal{U}_{3B}}{\partial y} \\ a_z &= -\frac{\partial \mathcal{U}_{3B}}{\partial z} \end{aligned} \tag{20}$$

which, together with Equations 16 to 18, yield the final output:

$$\begin{aligned} a_{U3B} &= \{a_x, a_y, a_z\} \\ a_x &= -\mu\left(\frac{-1+x}{(1-2x+x^2+y^2+z^2)^{\frac{3}{2}}}\right. \\ &\quad \left. - \frac{3x^2}{(x^2+y^2+z^2)^{\frac{5}{2}}} + \frac{1-x}{(x^2+y^2+z^2)^{\frac{3}{2}}}\right) \\ a_y &= -y\left(\frac{\mu}{(1-2x+x^2+y^2+z^2)^{\frac{3}{2}}}\right. \\ &\quad \left. - \frac{\mu(3x+x^2+y^2+z^2)}{(x^2+y^2+z^2)^{\frac{5}{2}}}\right) \\ a_z &= -z\left(\frac{\mu}{(1-2x+x^2+y^2+z^2)^{\frac{3}{2}}}\right. \\ &\quad \left. - \frac{\mu(3x+x^2+y^2+z^2)}{(x^2+y^2+z^2)^{\frac{5}{2}}}\right) \end{aligned} \tag{21}$$

3.3 Final Framework

Considering the two main reference frames involved (inertial on the GVE equations, Earth-pointing for the accelerations), some transformations have to be taken into account. The accelerations in Equation 4 have to be written in the Local Vertical, Local Horizontal frame (LVLH), which require the following transformation matrices [13]:

$$\begin{aligned} a_{LVLH} &= (R_E R R_F)^{-1}\big(a_{U3B} + a_{LT}\big) \\ R &= R_\Omega R_i R_\omega \end{aligned}$$

$$\begin{aligned} R_\Omega &= \begin{bmatrix} \cos\Omega & -\sin\Omega & 0 \\ \sin\Omega & \cos\Omega & 0 \\ 0 & 0 & 1 \end{bmatrix}, R_i = \begin{bmatrix} 1 & 0 & 0 \\ 0 & \cos i & -\sin i \\ 0 & \sin i & \cos i \end{bmatrix} \\ R_\omega &= \begin{bmatrix} \cos\omega & -\sin\omega & 0 \\ \sin\omega & \cos\omega & 0 \\ 0 & 0 & 1 \end{bmatrix}, R_F = \begin{bmatrix} \cos\nu & -\sin\nu & 0 \\ \sin\nu & \cos\nu & 0 \\ 0 & 0 & 1 \end{bmatrix} \\ R_E &= \begin{bmatrix} \cos(\nu_\oplus + \nu_\oplus^0) & \sin(\nu_\oplus + \nu_\oplus^0) & 0 \\ -\sin(\nu_\oplus + \nu_\oplus^0) & \cos(\nu_\oplus + \nu_\oplus^0) & 0 \\ 0 & 0 & 1 \end{bmatrix} \end{aligned} \tag{22}$$

Finally, Equations 4 are fully defined and the reference frame changes required by the algorithm are set. For a better understanding of the transformations involved and the overall framework, Figure 3 can be analysed.

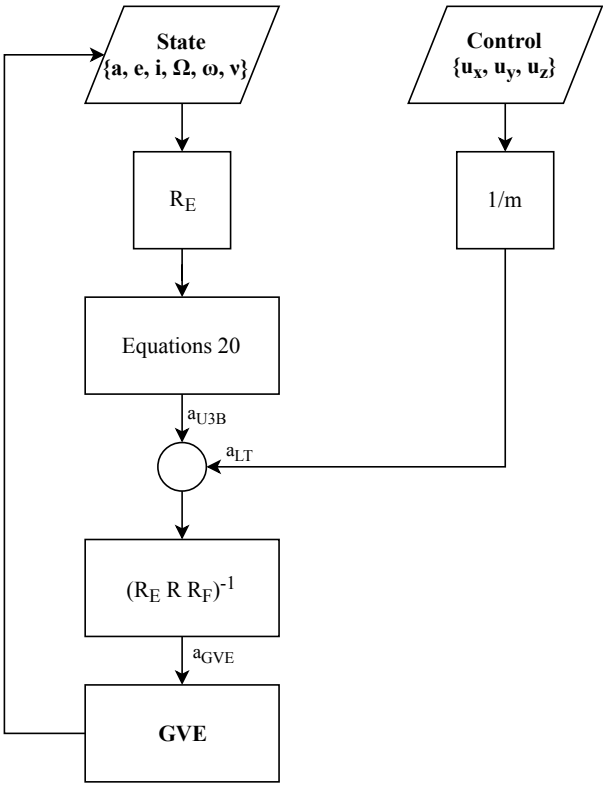

Fig. 3: Flow diagram of the state propagation using the GVE Framework, including matrix rotations

4. Low-Thrust Trajectory Design

In order to test the GVE equations in a mission design scenario, a simple asteroid capture case was devised. The mission entails coupling a spacecraft to a NEA and using electrical propulsion to change the body's nominal orbit, so that it will move into one of the manifolds of the Sun-Earth system. The considered spacecraft is akin to the one used by NASA's Asteroid Redirect Robotic Mission concept [14], with a dry mass of 5,500 kg and a maximum thrust capability of 2 N.

The low-thrust asteroid capture design will involve the following stages: first, the trajectory inserting the body into the invariant manifold orbit is computed, using impulsive manoeuvres. Then, the obtained Δv and time of flight are used to generate a first guess of the accelerated trajectory. This could be used to set up an optimal control problem that optimises the spacecraft's mass; however, since the purpose of this paper is to highlight the use

of the GVE equations, this latter step will not be shown here.

4.1 Preliminary Impulsive Trajectory

Designing the optimal impulsive transfer from a starting point to a target requires the optimisation of a Lambert arc. This trajectory is then differentially corrected into the third-body perturbed motion, using the GVE framework.

4.1.1 Lambert Arc Optimisation

The Lambert arc optimisation problem is here tackled by EPIC [15], a global trajectory optimiser. EPIC performs domain decomposition, where each domain is evaluated based on the evolution of a population of agents; its purpose is to generate a series of very good local optima instead of a global one, such that there is more flexibility to the mission design.

The earliest and latest dates for the transfer to occur were set as the beginning of 2036 and 2038, respectively. These were chosen in order for the transfer to cross the perturbation region defined in Sub-section 2.2, so that the advantage from using the GVE equations is highlighted. Between these two threshold points, EPIC finds the optimal initial and final conditions for the Lambert arc, computed in the two-body problem with zero revolutions and targeting a single manifold orbit of $C = 3$. These conditions are propagated from the threshold points using the GVE equations.

4.1.2 Differential Correction

Given that the Lambert arc is computed in the two-body problem model, it is necessary to find its equivalent using the method presented in this paper. This is done by employing a differential corrector to correct the Δv manoeuvres of the Lambert arc, so that an adjusted transfer will end up at the desired final state x_f in the presented GVE framework [16]. Considering a given reference trajectory, in which Φ is the state-transition matrix:

$$\begin{aligned} \dot{x} &= f(x(t)) \\ \delta x(t_1) &= \Phi(t_1, t_0)\delta x(t_0) \end{aligned} \tag{23}$$

The propagation of the state transition matrix is described by the following:

$$\begin{aligned} \delta\dot{x}(t) &= Df(x(t))\delta x \\ \dot{\Phi} &= Df(x(t))\Phi \end{aligned} \tag{24}$$

The Jacobian $Df(x(t))$ is defined by:

$$Df(x(t)) = \begin{bmatrix} 0 & 0 & 0 & 1 & 0 & 0 \\ 0 & 0 & 0 & 0 & 1 & 0 \\ 0 & 0 & 0 & 0 & 0 & 1 \\ a_{xx} & a_{xy} & a_{xz} & 0 & 0 & 0 \\ a_{yx} & a_{yy} & a_{yz} & 0 & 0 & 0 \\ a_{zx} & a_{zy} & a_{zz} & 0 & 0 & 0 \end{bmatrix} \tag{25}$$

which, using Hamiltonian dynamics, can be computed with:

$$\begin{aligned} a_{xx} = -\frac{\partial^2 \mathcal{H}_{3B}}{\partial x^2}, a_{yy} = -\frac{\partial^2 \mathcal{H}_{3B}}{\partial y^2}, a_{zz} = -\frac{\partial^2 \mathcal{H}_{3B}}{\partial z^2} \\ a_{xy} = a_{yx} = -\frac{\partial^2 \mathcal{H}_{3B}}{\partial x \partial y}, a_{yz} = a_{zy} = -\frac{\partial^2 \mathcal{H}_{3B}}{\partial y \partial z} \end{aligned} \tag{26}$$

4.2 Low-Thrust First Guess

The final low-thrust transfer will be represented by a state vector of the position, velocity, thrust and mass of the spacecraft throughout its duration. Some of its parameters are fixed: the initial and final points for the motion are the same as the Lambert arc. Then, the impulsive manoeuvre design is used to estimate the spacecraft's initial mass and transfer time using Tsiolkovsky's equation.

With these considerations, an optimisation procedure is devised to compute the transfer. Its goal is to minimize the error between the final transfer parameters and the target state, using the GVE framework presented in Figure 3 as the model of motion. The trajectory consists of two maximum thrust phases, interleaved with two coasting ones. Thus, the optimisation variables are simply the elevation, azimuth and duration of the thrust for each of the accelerated segments of motion. The optimisation is solved using MATLAB's *fmincon* routine.

As mentioned in Section 4, this paper concerns only this first guess design. Posteriorly, this could be used to set up an optimal control problem to maximise the total mass of the system or diminish the overall fuel cost, using the GVE framework for a straightforward definition of the motion's boundaries and constrains.

5. Case Study: Capture of Asteroid 2018 AV2

As of July 2018, more than 18,000 NEA have been discovered and listed on the Minor Planet Center Database [19]. From this pool, about 3,500 are boulder-sized asteroids (<30m diameter), which makes them potential candidates for low-thrust retrieval [10].

One of these is asteroid 2018 AV2. Given its discovery in January 2018, there is almost no data regarding its composition and nature. Nevertheless, this object is clearly

Table 1: Basic characteristics and estimates for Apollo asteroid 2018 AV2

Asteroid	Initial Capture Date	Final Capture Date	H	Diameter [m]*	Mean Mass [t]*
2018 AV2	2036/02/05	2037/08/07	28.7	[3.4 - 10.8]	[259 - 941]

* Obtained using near-Earth asteroids estimation models [17, 18]

moving in a low energy regime, making it a great candidate to test the accuracy and use of the GVE framework. Its next close approach to the Earth will happen in 2037, when it could be captured into a LPO. Table 1 presents some of its characteristics, together with the initial and final dates of the computed capture Lambert arc.

5.1 Preliminary Accuracy Analysis

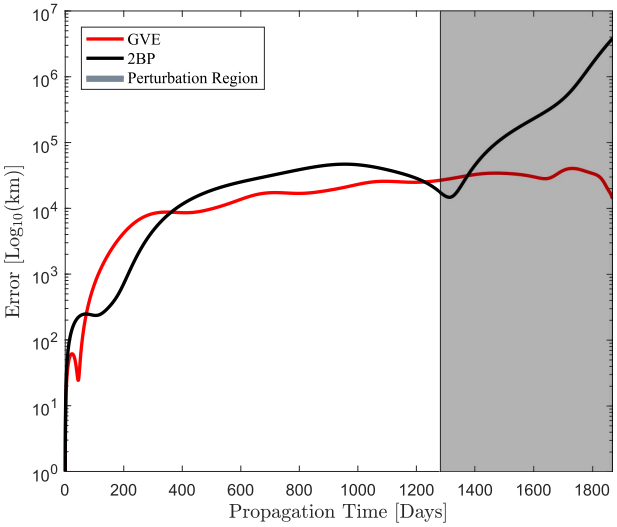

Fig. 4: Absolute position error as a function of time, compared to the CR3BP

Although the two-body problem remains a very common model for low-thrust transfers [20], it is extremely inaccurate in the intended trajectory design region. On the other hand, the GVE framework can be used to model motion up until very close to the Earth's sphere of influence, including the low-energy regime studied in Sub-section 2.2.

In order to carry out a quick comparison of how these two different models perform for the trajectory design in question, both were used to propagate the asteroid's motion in time, from a fixed point in space. In the synodic reference frame, the starting point of the motion corresponds to the crossing of the trajectory with the positive y-axis; the propagation ends when the motion reaches the positive x-axis (closest point to the Earth). The position errors are depicted in Figure 4, where it can clearly be seen that inaccuracies related to the two-body problem are especially high when entering the perturbation region, where the error surpasses the 10^6 km mark.

5.2 Asteroid Capture Trajectory

The low-thrust trajectory designed with the process described in Section 4 can be seen in Figure 5. The spacecraft captures the asteroid in the beginning of the red trajectory, and the thrusting phase ends at the manifold insertion point. It can be seen that this motion happens partially in the perturbation region described in Sub-section 2.2, something that could not be accurately computed using a lower-fidelity model.

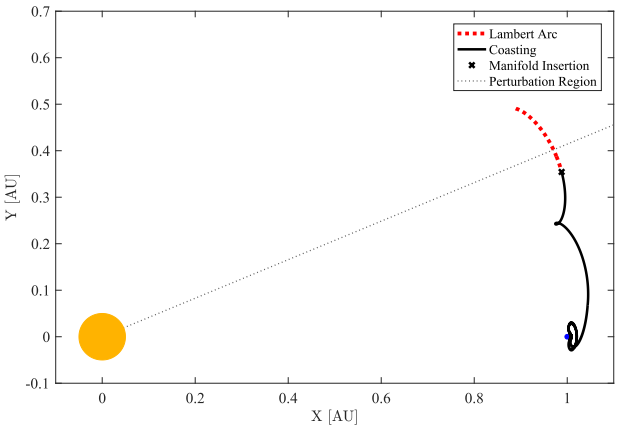

Fig. 5: Schematic of the first guess capture trajectory for asteroid 2018 AV2, ending at the manifold insertion point

The limits of the red trajectory were found by EPIC as the initial and final points of the optimal Lambert arc. The motion was then differentially corrected using the GVE framework, yielding a total Δv of 136.40 m.s^{-1}.

Using this preliminary trajectory, the obtained initial mass was, using Tsiolkovsky's equation, 696 tonnes. The procedure described in Sub-section 4.2 yielded the thrust profile for this first guess design, which is depicted in Figure 6. Two short thrust phases can be seen, in a on-off control scheme. Thus, as previously stated, the system's initial mass could actually be increased by using an op-

timal control solver, which would certainly optimise the thrust phases in Figure 6.

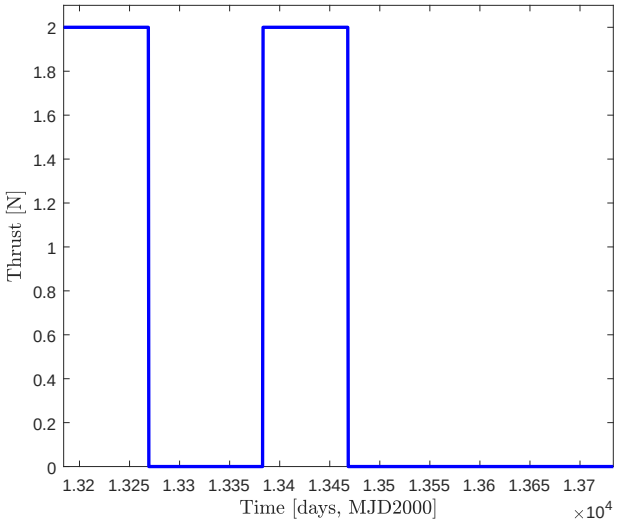

Fig. 6: Thrust profile of the first guess capture trajectory for asteroid 2018 AV2

6. Conclusions

This paper presents a novel formulation of the third-body perturbation, ideal for a GVE approach to the propagation of trajectories within low-energy regions and subject to low-thrust propulsive accelerations. This is particularly useful for mission design in low-energy regimes, where the simultaneous perturbation of both primaries cannot be approximated by a lower fidelity method.

The nature of the GVE equations makes them very advantageous for low-thrust trajectory design. Particularly, the intuitive observation of the orbital elements evolution and the easy definition of boundaries and constraints for the optimal control problem make the GVE framework straightforward to set up and solve, as opposed to methods like the CR3BP.

The developed equations of motion are valid for planetary systems with gravitational parameters of orders of magnitude similar to the Sun-Earth one. This makes them ideal for, among others, the computation of low-thrust trajectories for Jovian or Saturnian moon tours or near-Earth asteroid capture missions to LPOs. In the latter case, the trajectory design can target the invariant manifold structures very close to the periodic orbit, given the accuracy of the GVE framework up until very close to the Earth's sphere of influence.

Future work will deal with the implementation of the optimal control problem and mass optimisation of the asteroid trajectory. Furthermore, given the existence of singularities for the inclination and longitude of the ascending node elements in the GVE equations, an application of modified orbital elements is envisaged.

Acknowledgements

R.N. would like to acknowledge the support of the Amelia Earhart Fellowship grant and the Coachmakers' Eric Beverley Bursary.

References

[1] M. D. Rayman and D. H. Lehman, "Deep Space One: NASA's First Deep-Space Technology Validation Mission," 1997.

[2] M. Noton, "Low Thrust Missions," in *Spacecraft Navigation and Guidance*, pp. 125–140, Springer, 1998.

[3] B. Dachwald, "Low-thrust trajectory optimization and interplanetary mission analysis using evolutionary neurocontrol," *Doktorarbeit, Institut für Raumfahrttechnik, Universität der Bundeswehr, München*, 2004.

[4] I. M. Ross and F. Fahroo, "A Perspective on Methods for Trajectory Optimization," in *AIAA/AAS Astrodynamics Specialist Conference and Exhibit*, p. 4727, 2002.

[5] A. Shirazi, J. Ceberio, and J. A. Lozano, "Spacecraft trajectory optimization: A review of models, objectives, approaches and solutions," *Progress in Aerospace Sciences*, 2018.

[6] S. D. Ross and D. J. Scheeres, "Multiple Gravity Assists, Capture, and Escape in the Restricted Three-Body Problem," *SIAM Journal on Applied Dynamical Systems*, vol. 6, no. 3, pp. 576–596, 2007.

[7] E. M. Alessi and J. P. Sánchez, "Semi-Analytical Approach for Distant Encounters in the Spatial Circular Restricted Three-Body Problem," *Journal of Guidance, Control, and Dynamics*, vol. 39, no. 2, pp. 351–359, 2015.

[8] W. S. Koon, M. W. Lo, J. E. Marsden, and S. D. Ross, "Low Energy Transfer to the Moon," *Celestial Mechanics and Dynamical Astronomy*, vol. 81, no. 1-2, pp. 63–73, 2001.

[9] D. Nesvornỳ, D. Vokrouhlickỳ, and A. Morbidelli, "Capture of Irregular Satellites during Planetary Encounters," *The Astronomical Journal*, vol. 133, no. 5, p. 1962, 2007.

[10] J. P. Sánchez, R. Neves, and H. Urrutxua, "Trajectory Design for Asteroid Retrieval Missions: A Short Review," *Frontiers in Applied Mathematics and Statistics [in publication]*, 2018.

[11] V. Szebehely and E. Grebenikov, "Theory of Orbits - The Restricted Problem of Three Bodies.," *Soviet Astronomy*, vol. 13, p. 364, 1969.

[12] J. P. Sánchez and D. G. Yárnoz, "Asteroid Retrieval Missions enabled by Invariant Manifold Dynamics," *Acta Astronautica*, vol. 127, pp. 667–677, 2016.

[13] R. H. Battin, *An Introduction to the Mathematics and Methods of Astrodynamics*. American Institute of Aeronautics and Astronautics, 1999.

[14] J. Brophy, F. Culick, L. Friedman, C. Allen, D. Baughman, J. Bellerose, and et al., "Asteroid Retrieval Feasibility Study," report, Keck Institute for Space Studies, Califonia Institute of Technology, Jet Propulsion Laboratory, 2012.

[15] M. Vasile and M. Locatelli, "A Hybrid Multiagent Approach for Global Trajectory Optimization," *Journal of Global Optimization*, vol. 44, no. 4, pp. 461–479, 2009.

[16] W. Koon, M. Lo, J. Marsden, and S. D. Ross, "Dynamical Systems, the Three-Body Problem and Space Mission Design," *Free online Copy: Marsden Books*, 2008.

[17] E. Bowell, B. Hapke, D. Domingue, K. Lumme, J. Peltoniemi, and A. Harris, "Application of photometric models to asteroids," in *Asteroids II*, pp. 524–556, 1989.

[18] S. Chesley, P. Chodas, A. Milani, G. Valsecchi, and D. Yeomans, "Quantifying the Risk posed by Potential Earth Impacts," *Icarus*, vol. 159, no. 2, pp. 423–432, 2002.

[19] "Minor Planet Center Asteroid Database." `http://www.minorplanetcenter.net/iau/TheIndex.html`, 2017. Accessed: 2017-07-11.

[20] S. Tang and B. A. Conway, "Optimization of Low-Thrust Interplanetary Trajectories using Collocation and Nonlinear Programming," *Journal of Guidance, Control, and Dynamics*, vol. 18, no. 3, pp. 599–604, 1995.

Gauss' variational equations for low-thrust optimal control problems in low-energy regimes

Neves, Rita

2018-10-05

Rita Neves and Joan Pau Sanchez Cuartielles. Gauss' variational equations for low-thrust optimal control problems in low-energy regimes. Proceedings of the International Astronautical Congress 2018 (IAC '18), 1-5 October 2018, Bremen, Germany.

https://iafastro.directory/iac/archive/